Conclusions

The time domain code ASSPIN provides acousticians with a powerful method of advanced propeller noise prediction. With the exception of nonlinear effects, the code utilizes exact solutions of the Ffowcs Williams-Hawkings equation with exact blade geometry and kinematics. With the inclusion of nonaxial inflow, periodic loading noise, and adaptive time steps to speed up computer execution, the development of this code is now complete. It is important to recognize that correct blade coordinates and loads must be obtained by iteration between an aeroelastic and an aerodynamic code. In addition, the effects of other acoustic phenomena, such as reflections from wing, nacelle, and fuselage, in aircraft tests must be included in comparisons of measured and predicted noise data.

References

[1]Nallasamy, M., Envia, E., Clark, B. J., and Groeneweg, J. F., "Near-Field Noise of a Single Rotation Propfan at an Angle of Attack," AIAA Paper 90-3953, Oct. 1990.

[2]Hanson, D. B., "Near-Field Frequency-Domain Theory for Propeller Noise," *AIAA Journal,* Vol. 23, No. 4, 1985, pp. 499–504.

[3]Hanson, D. B., "Unified Aeroacoustic Analysis for High Speed Turboprop Aerodynamics and Noise," NASA CR-4329, March 1991.

[4]Bartel, H. W., and Swift, G., "Near-Field Acoustic Characteristics of a Single-Rotor Propfan," AIAA Paper 89-1055, April 1989.

[5]Hanson, D. B., "Noise Radiation of Propeller Loading Sources with Angular Inflow," AIAA Paper 90-3955, Oct. 1990.

[6]Hanson, D. B., "Direct Frequency Domain Calculation of Open Rotor Noise," *AIAA Journal,* Vol. 30, No. 9, 1992, pp. 2334–2337.

[7]Farassat, F., and Succi, G. P., "The Prediction of Helicopter Rotor Discrete Frequency Noise," *Vertica,* Vol. 7, No. 4, 1983, pp. 309–320.

[8]Farassat, F., "Theoretical Analysis of Linearized Acoustics and Aerodynamics of Advanced Supersonic Propellers," *Aerodynamics and Acoustics of Propellers,* AGARD CP-366(10), 1985, pp. 1–15.

[9]Farassat, F., Padula, S. L., and Dunn, M. H., "Advanced Turboprop Noise Prediction Based on Recent Theoretical Results," *Journal of Sound and Vibration,* Vol. 119, 1987, pp. 53–79.

[10]Celestina, M. L., Mulac, R. A., and Adamczyk, J. J., "A Numerical Simulation of the Inviscid Flow Through a Counter-Rotating Propeller," *Transactions of the ASME, Journal of Turbomachinery,* Vol. 108, 1986, pp. 187–193.

[11]Spence, P. L., "Development of a Boundary Layer Noise Propagation Code and Its Application to Advanced Propellers," AIAA Paper 91-0593, Jan. 1991.

[12]Dunn, M. H., and Farassat, F., "High-Speed Propeller Noise Prediction—A Multidisciplinary Approach," *AIAA Journal,* Vol. 30, No. 7, 1992, pp. 1716–1723; also AIAA Paper 90-3934.

Comparison of Transonic Flow Models

Kevin McGrattan*
New York University, New York, New York 10003

Introduction

DURING the past 10 years, there has been much discussion of the relative merits of the potential and the Euler formulations of the equations of motion of transonic flow over supercritical wing sections. To study the two models in a common framework, a finite difference version of the Euler solver[1] has been incorporated into the potential code that is described in Ref. 2. The purpose of this Note is to highlight some of the more interesting discoveries of the study.

First, the Euler solver is less reliable than the potential solver in predicting the wave drag. For computations of the Euler equations with a boundary-layer correction, the standard pressure integration around the airfoil is faulty due to the inaccuracy of the flow variables in the wake. As a possible alternative, the Euler equations modified by artificial viscosity terms can be combined to form an equation for the entropy whose viscous terms provide a means of calculating the wave drag. Instead of differencing uncertain values of pressure at the tail and the nose, a positive definite quantity is integrated over the region surrounding a shock.

For flows with relatively weak shocks, there is little difference between the Euler and the potential models because the jump in entropy across a shock is of third order in the shock strength. This suggests that in cases with weak shocks, there should exist nonunique solutions of the Euler equations where there exist nonunique solutions of the potential equations. References 3 and 4 present nonunique solutions of the potential equation for airfoils at relatively high Mach numbers with strong shocks. The authors claim that the phenomenon is related to the isentropic assumption of the potential model. However, a thin, supercritical airfoil will be presented which not only yields a nonunique potential solution, but also a nonunique Euler solution.

Wave Drag and the Entropy Inequality

The Euler solver described in Ref. 1 employs central differences for all spatial derivatives, and therefore explicit artificial viscosity terms must be added to all four equations in order to guarantee convergence. A check on the physical validity of the additional terms is to show that the entropy inequality is satisfied by the modified equations. From this an alternative method of computing wave drag may be derived following the idea presented in Ref. 5. This calculation involves the summing of a positive definite quantity over the region of the flow in which the shock is smeared, avoiding the use of computed flow variables near the tail which are subject to great uncertainty when a boundary-layer correction is included.

Consider the Euler equations modified by the second-order artificial viscosity terms:

$$\rho_t + (\rho u)_x + (\rho v)_y = \nabla \cdot \nu \nabla \rho \tag{1a}$$

$$(\rho u)_t + (\rho u^2 + p)_x + (\rho uv)_y = \nabla \cdot \nu \nabla (\rho u) \tag{1b}$$

$$(\rho v)_t + (\rho uv)_x + (\rho v^2 + p)_y = \nabla \cdot \nu \nabla (\rho v) \tag{1c}$$

$$(\rho E)_t + (\rho uH)_x + (\rho vH)_y = \nabla \cdot \nu \nabla (\rho H) \tag{1d}$$

where the artificial viscosity operator is defined as

$$\nabla \cdot \nu \nabla \equiv \frac{\partial}{\partial x}\left(\nu^{(x)}\frac{\partial}{\partial x}\right) + \frac{\partial}{\partial y}\left(\nu^{(y)}\frac{\partial}{\partial y}\right)$$

These four equations may be combined to form a fifth equation for the entropy

$$(\rho S)_t + (\rho uS)_x + (\rho vS)_y = \frac{c_v \rho}{e}\|w\|^2_{WD} + \nabla \cdot \nu\left\{S\nabla\rho + \frac{c_v \rho \nabla e}{e} + \frac{c_v \nabla p}{e}\right\} \tag{2}$$

The positive definite wave-drag norm is defined as

$$\|w\|^2_{WD} = \|\nabla u\|^2 + \|\nabla v\|^2 + \gamma e\left(\left\|\frac{\nabla p}{p}\right\|^2 - \frac{\gamma+1}{\gamma}\left\langle\frac{\nabla p}{p}, \frac{\nabla \rho}{\rho}\right\rangle + \left\|\frac{\nabla \rho}{\rho}\right\|^2\right)$$

Received Sept. 17, 1991; revision received Dec. 16, 1991; accepted for publication Dec. 17, 1991.

*Courant Institute of Mathematical Sciences; currently at National Inst. of Standards and Technology, Gaithersburg, MD 20899.

where the inner product $\langle \cdot, \cdot \rangle$ is defined like the preceding artificial viscosity operator.

In steady state, Eq. (2) may be integrated over a region of the flow domain D, and following an application of the divergence theorem, it becomes

$$\oint_{\partial D} \rho S q \cdot n \, dl = \iint_D \frac{c_v \rho}{e} \| w \|^2_{WD} \, dx \, dy + \oint_{\partial D} \nu \{ S \nabla \rho + \cdots \} \cdot n \, dl \tag{3}$$

To prove that the modified Euler equations satisfy the entropy inequality, take D to be the arbitrarily narrow strip of width ϵ surrounding a shock. As $\nu \to 0$, the second integral on the right-hand side disappears since the integrand is bounded on each side of the shock. The remaining equation asserts that the jump in entropy across a shock is positive.

Equation (3) may be used again to derive a formula for the wave drag. Taking D to be the entire flow domain, the left-hand side reduces to an integration at infinity due to the no flux boundary condition, $q \cdot n = 0$. The second integral on the right-hand side may be neglected since ν is small and the normal derivatives of the relevant flow variables remain bounded. Thus the equation

$$\oint_{\infty} \rho S q \cdot n \, dl = \iint_D \frac{c_v \rho}{e} \| w \|^2_{WD} \, dx \, dy \tag{4}$$

provides a convenient formula for calculating the wave drag. Its coefficient is given by the momentum flux integral

$$C_{WD} = \frac{-2}{\rho_\infty q_\infty^2} \oint_{\infty} (\rho u q \cdot n + p n_x) \, dl \tag{5}$$

where n_x is the x component of the outward-facing normal along any simple, closed contour enclosing the airfoil.

Let the freestream conditions be $u_\infty = 1$, $v_\infty = 0$, $p_\infty = 1$, and $\rho_\infty = \gamma M_\infty^2$. It is assumed that p and ν recover their freestream values in the narrow strip of particle paths extending from the back of the shock to infinity, but that ρ and u do not. Bernoulli's law allows u to be written solely as a function of the entropy S where

$$u = \sqrt{1 + 2\gamma e_\infty \left\{ 1 - \exp\left(\frac{S - S_\infty}{\gamma c_v} \right) \right\}} \tag{6}$$

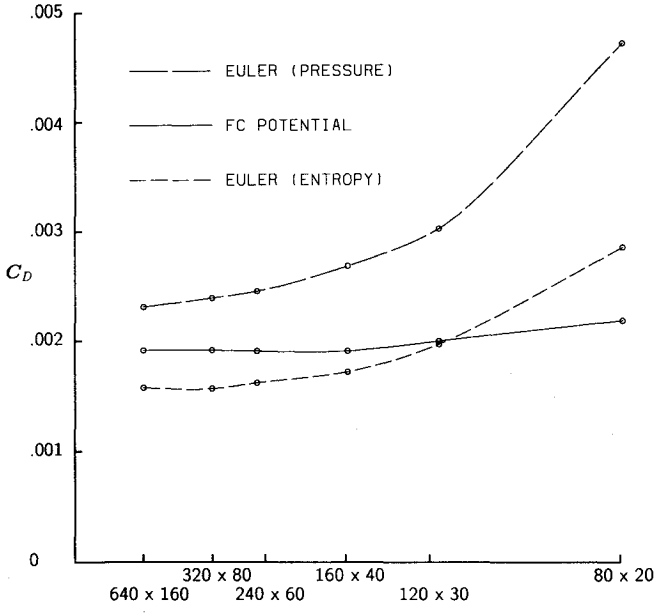

Fig. 1 Convergence study for wave-drag calculations.

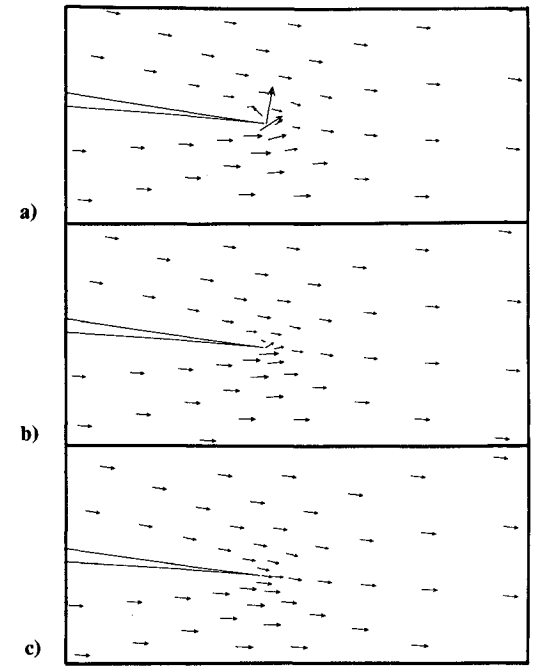

Fig. 2 Vortex: a) formation at the trailing edge, b) partial suppression, and c) complete suppression.

To first order in ΔS, this yields the relation

$$u_\infty (u - u_\infty) = (-e_\infty / c_v)(S - S_\infty) \tag{7}$$

Now the preceding drag formula (5) may be rewritten in terms of the entropy gain across the shock

$$C_{WD} = \frac{2 e_\infty}{\rho_\infty q_\infty^2 c_v} \oint_{\infty} \rho u (S - S_\infty) \, dy \tag{8}$$

This formula is presented by Oswatitsch.[6] For computational purposes, the entropy flux integral of Eq. (8) may be expressed in terms of the double integral of Eq. (4) computed over the region of the flow domain exhibiting large gradients in the flow variables, namely the neighborhood of the shock. Thus, finally

$$C_{WD} = \frac{2 e_\infty}{\rho_\infty q_\infty^2} \iint_D \frac{\rho}{e} \| w \|^2_{WD} \, dx \, dy \tag{9}$$

A convergence study for this new formula is presented in Fig. 1. Observe that for the NACA 0012 airfoil at zero angle of attack and Mach number $M = 0.78$, the wave-drag coefficient converges to a value of 0.0016, or 16 counts of drag. This value is lower than that of the fully conservative (FC) potential solver, which predicts 19.4 counts. This value is in turn lower than the Euler value that is predicted from the pressure integral, which appears to be heading towards about 22.5 counts.

Because the Euler and the FC potential solutions are virtually identical at this Mach number, their wave-drag coefficients should be the same as well. However, the Euler coefficient from the entropy formula (9) is lower due to the discretization error associated with the summation of the positive definite terms.[7] The wave drag from the presure integral converges to a value slightly higher than that of the potential scheme because of uncertainty in the pressure values in the wake. The errors are due to radial stretching and the extra artificial viscosity terms required to enforce the Kutta-Joukowski condition, which will be described next.

Euler Nonuniqueness

References 3 and 4 present nonunique solutions of the potential equation for cases in which the shocks are relatively

strong. It is claimed that the cause of this phenomenon is the isentropic assumption. However, in cases of weak shocks, the main difference between the FC potential and the Euler models is not the isentropic assumption but rather the treatment of the Kutta-Joukowski condition. The potential model explicitly restricts the flow from turning around the trailing edge, and the velocity potential throughout the entire flowfield is readjusted at each iteration to account for the new value of circulation about the airfoil. The Euler solver does not have a similar mechanism of enforcing the Kutta-Joukowski condition.

Instead, the Euler solver relies on higher-order artificial viscosity terms to restrict the flow from turning around the trailing edge. Consider the modified Euler equations written in idealized form

$$w_t + f(w)_x + g(w)_y = \nabla \cdot \nu_2 \nabla w - \nabla \cdot \nu_4 \nabla \Delta w \qquad (10)$$

The second-order terms of the artificial viscosity are needed to satisfy the entropy inequality in the neighborhood of a shock, where the coefficient ν_2 is of first order in the grid spacing. The fourth-order terms, whose coefficient ν_4 is of third order, are not only needed to stabilize the computation in the far field, but also to suppress vortices at the trailing edge.

Figure 2a displays the flowfield that is established at the trailing edge after only 19 iterations. This flow pattern resembles those of actual physical experiments in which a small vortex forms just above the trailing edge of the airfoil and is then shed off as circulation is established around the airfoil. Unfortunately, the computation fails during the next iteration because of the cavitation created by a rapid increase in the flow velocity around the tail of the airfoil. In Fig. 2b, after the viscosity parameter ν_4 is increased, the vortex is suppressed, and in Fig. 2c disappears after the value is increased even further.

Also unlike the potential solver, the Euler solver also has no simple way of adjusting the flow variables to account for changes in the circulation around the airfoil other than through the propagation of the information into the flowfield from the solid and far-field boundaries. To imitate the potential solver as much as possible, a far-field boundary condition has been included in the Euler routine which adds a circulation to the freestream velocity vector.[8] In addition, the circulation is relaxed in the far field to favor the existing circulation established by the potential initialization. In this way the drastic loss of lift is prevented during the time lag required to propagate the updated circulation into the flowfield.

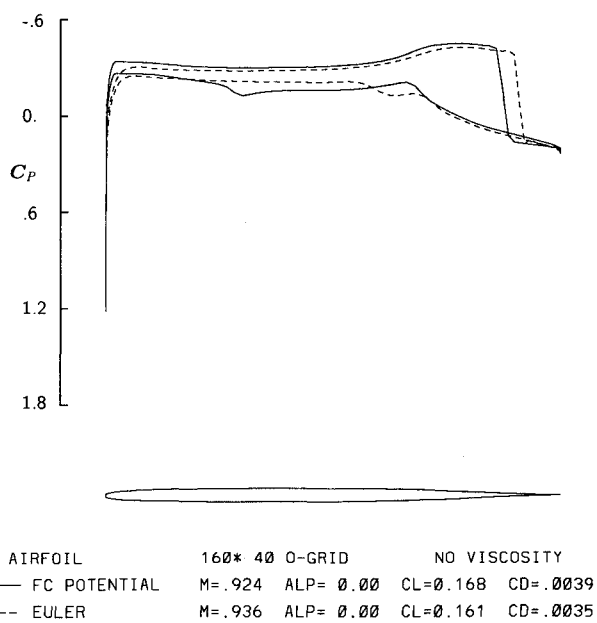

Fig. 3 Nonunique solutions to both the potential and Euler equations for a 3% thick symmetric airfoil.

A thin, shockless airfoil that yields nonunique solutions of both the potential and the Euler equations was designed using the method of complex characteristics.[9] The objective was to find an airfoil that gives rise to a large supersonic zone and relatively weak shocks at high Mach numbers. Remarkably, the potential solver yields a nonunique solution at the design Mach number; and this nonunique solution is used as an initialization of the Euler computation. The Euler solver does not yield nonunique solutions as easily as the potential, and it is difficult to determine just the right set of parameters which do the job. Figure 3 displays the results. The Euler solver yields a nonunique solution for a Mach number slightly above design. The Euler residual, the root mean square of the quantity $\partial\rho/\partial t$, was reduced to the order of 10^{-6}. The wave drag in both cases is low, suggesting that the nonuniqueness has more to do with the implementation of the Kutta-Joukowski condition than the isentropic assumption.

Conclusions

The alternative wave-drag calculation for the Euler solver serves two purposes. First, the existence of the positive definite term in the entropy conservation equation (2) verifies that the Jameson Euler scheme satisfies the entropy inequality. Second, this equation may be integrated over the entire flow domain to yield the wave drag on the airfoil. In a two-dimensional computation this method is faulty due to truncation error; however, for a three-dimensional computation it might serve as a useful tool in isolating the wave drag from the larger induced drag. In either case, the idea is to look directly at the shock for an assessment of its severity, rather than to rely on a pressure integration about the airfoil.

The need to dissipate vorticity in the wake region necessitates the addition of higher-order artificial viscosity terms. This fact has repercussions for both the wave-drag computation and the nonuniqueness question. First, the addition of extra terms in the wake calls into question the reliability of the pressure integral (5) as a measure of wave drag. Second, the explicit mechanism by which the potential solver enforces the Kutta-Joukowski condition yields, as an unwanted side effect, nonunique solutions for a certain range of Mach number. The fact that the Euler solver does not have a similar mechanism means that it will not as easily generate nonunique solutions. However, because the fully conservative potential and the Euler solutions are very similar in the presence of weak shocks, there is no reason why a nonunique potential solution with weak shocks should not have an Euler counterpart. Indeed, such a nonunique solution exists for a thin, symmetric airfoil. The exact cause of this phenomenon is yet to be determined, but it is unlikely that it is due to the isentropic assumption of the potential model.

Acknowledgments

This work has been partially supported by the Pittsburgh Supercomputing Center under Grant DMS-900024P, National Science Foundation Grant DMS-8922805, Department of the Air Force Grant AFOSR-91-0042, and U.S. Department of Energy Grant DE-FG02-88ER25053. I would like to thank my thesis advisor Paul Garabedian as well as Frances Bauer for their support of this work, especially for their contribution to the nonuniqueness problem.

References

[1]Jameson, A., Schmidt, W., and Turkel, E., "Numerical Solution of the Euler Equations by Finite Volume Methods Using Runge-Kutta Time-Stepping Schemes," AIAA 14th Fluid and Plasma Dynamics Conf., Palo Alto, CA, 1981.

[2]Bauer, F., Garabedian, P., Korn, D., and Jameson, A., "Supercritical Wing Sections II" *Lecture Notes in Economics and Mathematical Systems*, edited by M. Beckmann and H. P. Künzi, Vol. 108, Springer-Verlag, New York, 1975.

[3]Salas, M., Gumbert, C., and Turkel, E., "Nonunique Solutions to the Transonic Potential Flow Equation," *AIAA Journal*, Vol. 22, No. 1, 1984, pp. 145-146.

[4]Steinhoff, J., and Jameson, A., "Multiple Solutions of the Transonic Potential Flow Equations," *AIAA Journal*, Vol. 20, No. 11, 1982, pp. 1521-1525.

[5]Bauer, F., Garabedian, P., and Chang, I. C., "Wave Drag and the Entropy Inequality in Transonic Flow," *Advances in Computational Transonics* (to be published).

[6]Oswatitsch, K., *Gas Dynamics*, Academic Press, New York, 1956, Chap. 6.

[7]McGrattan, K., "A Comparison of the Potential and the Euler Formulations of the Equations of Transonic Flow," Ph.D. Thesis, New York Univ., New York, NY, 1991.

[8]Thomas, J., and Salas, M., "Far-Field Boundary Conditions for Transonic Lifting Solutions to the Euler Equations," *AIAA Journal*, Vol. 24, No. 7, 1986, pp. 1074-1080.

[9]Bledsoe, M., "The Method of Complex Characteristics for Design of Transonic Blade Sections," Research and Development Rept. DOE/ER/03077-273, New York Univ., New York, NY, June 1986.

High-Velocity Measurements via Laser Doppler Anemometer Using Single- and Multiaxial-Mode Lasers

J.-A. Wang* and C. L. Dancey†
Virginia Polytechnic Institute and State University, Blacksburg, Virginia 24061

Introduction

WHEN a multiaxial-mode laser is used in a laser Doppler anemometer (LDA) system the resulting signal contains distinct frequencies other than the Doppler frequency.[1] The other frequencies are the result of the Doppler signal "beating" with the axial modes of the laser. If the beat frequencies are close to the Doppler frequency, it may not be possible to separate them, by electronic filtering, for example. This problem is particularly relevant to high-velocity flows where Doppler frequencies may be comparable to the intermode frequency of the laser. The axial modes and related beat frequencies can be eliminated by installing a tuned etalon to achieve single axial-mode laser operation. Unfortunately, this results in a large loss in incident laser beam power, which is undesirable, particularly for high-velocity measurements.

Although the presence of "beat" frequencies in LDA signals has been experimentally verified, the impact they may have on validated LDA measurements has not been investigated. It is not clear that isolation of the Doppler frequency from the beat frequencies or elimination of the beat frequencies is necessary, in practice. To ascertain the practical effects of multiaxial-mode laser operation on LDA measurements, a sequence of experimental tests were run at relevant flow and LDA operating conditions. From these tests, it is concluded that the presence of the beat frequencies had no significant effect on the measured mean velocities. Data rates were in general higher during multimode operation and measured velocity fluctuation intensities were marginally lower without etalon mode selection.

Experimental Setup

A small-scale ($\sim 12\times \sim 15$-mm test section) wind tunnel with a nominal test section Mach number of 2 was used for the experiments. The tunnel was small enough to be run from a machine shop air supply. Measurements were made using the 514.5-nm channel of an argon-ion laser in a forward-scatter LDA system with counterbased processing and with 1% comparison tolerance for the rejection of noisy bursts. A single measurement was obtained per Doppler burst, based upon eight fringes with a total of 1024 measurements acquired per sample location. Polystyrene latex spheres of 0.54 μm diameter were used as the seed material for the tests.

The tests consisted of systematically varying the velocity at the LDA measurement volume by traversing the measurement volume along the axis of the tunnel. In this manner, a wide range of mean flow velocities and corresponding Doppler and beat frequencies were obtained. Measurements were made with and without an etalon installed (termed single-mode and multimode operation, respectively) and at two different laser power levels (0.5 and 1.2 W on all lines for single-mode operation; 1.0 and 2.0 W on all lines for multimode operation). Furthermore, a range of electronic filter bandwidths were successively applied at each location to assess the effects of selective filtering on the processed signal. The filter settings include low-limit/high-limit filter combinations of 65/200, 50/200, 20/200, and 10/200 MHz. The etalon was carefully tuned before initiating each set of tests.

Results

For the LDA used in the tests, the Doppler frequency ν_D and the beat frequency ν_B closest to the Doppler frequency vary with the flow velocity as indicated by the solid lines in Fig. 1. (Frequency in megahertz is given on the right axis for convenience.) ν_D and ν_B are widely separated for very low and very high velocities; but they are comparable and in fact pass through one another at a velocity of approximately 250 m/s. (The reference velocity used on the abscissa in both figures is the mean velocity in the tunnel obtained with etalon mode selection, at the maximum power of 1.2 W, and the narrowest permissible bandpass filter combination.) The electronic bandpass filter limits were such that, for multimode operation, at most one beat frequency was possible in the processed signal. All other beat frequencies were easily eliminated by the filters. In many cases, the filters eliminated all beat frequencies.

Figure 1 shows the mean velocity results (left axis) for both single and multimode operation at 1.2 and 2.0 W, respectively. The two groups of data form (within experimental error) two, slightly displaced, parallel lines. It was found that the laser power and, more importantly, filter bandwidth had no significant effect on the measured mean velocities for either group, and in order to simplify the graph these variables were not included in Fig. 1. The small displacement between the two groups of data is not associated directly with the operation of the etalon, but rather it is due to a change in alignment and orientation of the LDA that was required when the etalon was installed and tuned. Accounting for this fixed bias, there was

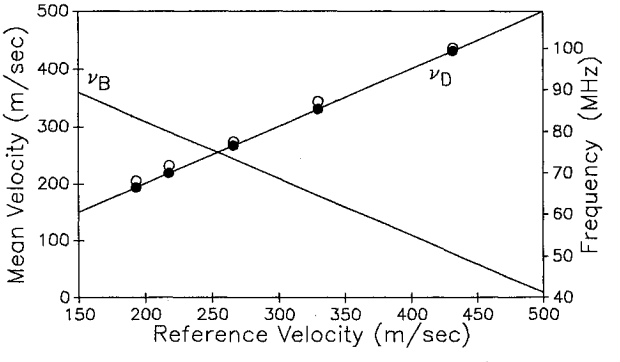

Fig. 1 Measured mean velocity (left axis) and Doppler and beat frequency (right axis) vs tunnel reference velocity, 50/200 MHz bandpass filter limits. •, 1.2 W, single mode; ○, 2.0 W, multimode.

Received Sept. 24, 1991; revision received Jan. 19, 1992; accepted for publication Feb. 10, 1992.

*Graduate Research Assistant, Department of Mechanical Engineering.

†Assistant Professor, Department of Mechanical Engineering. Member AIAA.